Convex Performance Envelope for Minimum Lap Time Energy Management of Race Cars

Pol Duhr, Ashwin Sandeep, Alberto Cerofolini, and Christopher H. Onder

***Abstract*—The optimization of the energy management of modern hybrid-electric or fully electric race cars for minimum lap time requires a description of the vehicle dynamics performance envelope, that is, of the tires' grip limit in corners, braking zones and during acceleration. In this paper, we present a computationally efficient performance envelope model in the form of convex constraints on the achievable longitudinal and lateral acceleration, on the assumption that the path on the track is given. The proposed acceleration limits are modeled velocity-dependent to take into account the effect of aerodynamic downforce present in many circuit race cars. The formulation as linear equality, inequality and second-order cone constraints allows to embed the model in a convex energy management optimization framework. To showcase the approach, we identify the model with data obtained from a state-of-the-art hybrid-electric Formula 1 car and present results for the Silverstone and Spa-Francorchamps circuits. The optimal energy management strategies can be evaluated with a computational time of less than 1 s. The optimal velocity profile subject to the performance envelope constraints is close to the measured one. The good agreement between the optimal solution and the measurement data shows that the proposed model captures the vehicle dynamics accurately enough for the purposes of energy management optimization.**

***Index Terms*—Energy management, Formula 1, hybrid electric, motor racing, optimal control, vehicle Dynamics.**

I. Introduction

MOTOR racing is all about lapping a given circuit in minimum time. Put simply, the driver should accelerate as hard as possible out of each corner and keep accelerating until braking as late as possible and decelerating just enough to negotiate the next corner at maximum possible speed and lateral acceleration. An intuitive manner to represent the driver and vehicle performance is the so-called *g-g diagram* [1]. An example is shown in Fig. 1 with measurement data of a professional driver in a Formula 1 (F1) car, which are the fastest circuit race cars. The diagram jointly represents the measured longitudinal and lateral acceleration. By Newton's second law, the total combined acceleration is proportional to the total friction force generated by all four tires. The race driver tries to bring the combined acceleration to the limit imposed by the tire forces whenever possible, subject to the vehicle dynamics, thereby operating at the boundary of the feasible space in the g-g diagram. We call this boundary the *performance envelope* of the race car. It can be seen that it is not constant, but varies with the velocity. Indeed, F1 cars are equipped with an aerodynamic package consisting of front and rear wings and a flat underbody, generating an aerodynamic downforce and thus a normal force on the tires that increases with velocity [2]. Hence, the friction limit of the tires and therefore the feasible acceleration increase - an effect exploited by many modern race cars. Given these observations, any attempt to compute the achievable lap time of a race car by simulation or optimization must include some mathematical model that captures its performance envelope.

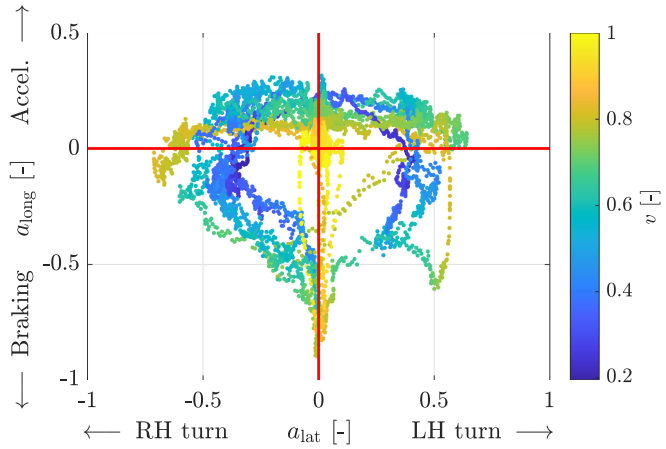

Fig. 1. g-g diagram of a contemporary F1 car, with the longitudinal acceleration a_{long} represented on the vertical axis and the lateral acceleration a_{lat} on the horizontal axis. The diagram is divided in four quadrants, corresponding to acceleration and braking combined with right-hand (RH) and left-hand (LH) cornering, respectively. The color-coding indicates the normalized velocity v.

The achievable longitudinal acceleration is not only determined by the tires' friction force, but also by the drag forces acting on the car and, most importantly, by the propulsive force that can be provided by its powertrain at any time on track. Recent years have seen many racing series move towards ever more complex powertrain architectures. The hybrid-electric F1 cars introduced in 2014 are certainly the most prominent example. As shown in Fig. 2, their so-called power unit is of a parallel-hybrid design and consists of a turbocharged internal combustion engine coupled to two electric motors: The motor-generator-unit-kinetic (MGU-K) is used for energy recuperation

Manuscript received 25 November 2021; revised 8 March 2022; accepted 27 April 2022. Date of publication 5 May 2022; date of current version 15 August 2022. The review of this article was coordinated by Dr. Hamid Taghavifar.*(Corresponding author: Pol Duhr.)*

Pol Duhr, Ashwin Sandeep, and Christopher H. Onder are with the Institute for Dynamic Systems and Control, ETH Zürich, 8092 Zürich, Switzerland (e-mail: pduhr@idsc.mavt.ethz.ch; asandeep@ethz.ch; onder@idsc.mavt.ethz.ch).

Alberto Cerofolini is with the Power Unit Performance and Control Group, Ferrari S.p.A., 41053 Maranello, Italy (e-mail: alberto.cerofolini@ferrari.com).

Digital Object Identifier 10.1109/TVT.2022.3172473

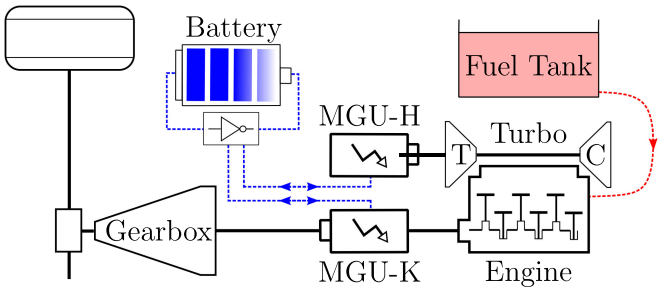

Fig. 2. Schematic of the mechanical and electrical components of the hybrid electric F1 power unit, showing the turbocharged internal combustion engine and the two electric motor-generator units MGU-K and MGU-H. Beside the fuel tank, energy can be drawn from or stored in the battery. Propulsive power is transmitted to the rear wheels via the gearbox.

in braking phases, to enable engine load-point shifting [3] and to boost in acceleration phases. The motor-generator-unit-heat (MGU-H) is coupled to the turbocharger shaft. It mainly recuperates excessive power generated by the turbine, but can also accelerate the turbocharger compound to reduce turbo lag. Both MGUs are connected to the battery, which serves as an energy storage. The technical regulations [4] impose strict limits on the fuel and battery energy consumption during a race, thereby creating the need for a supervisory energy management controller that coordinates all the power flows. Considering these restrictions and the complexity of the powertrain, the energy management strategies must be carefully optimized for minimum lap time. The same considerations are valid for other race cars with energy consumption limits, such as hybrid-electric Le Mans Hypercars [5] and electric Formula E cars [6].

Against this background, our paper proposes a set of convex constraints that model the performance envelope of a race car and can be included in a computationally efficient energy management optimization framework.

A. *Literature Review*

We identify four relevant fields of research pertaining to the topic of minimum-lap-time energy management optimization. The first one concerns the aforementioned g-g diagram. It was identified as a simple but suitable manner to analyze driver and vehicle performance [1] and to represent a race car's performance envelope [7]. The practical applications of the g-g diagram are very diverse, ranging from driver models [8] to vehicle stability controllers [9], the analysis of a limited slip differential's impact on vehicle dynamics [10], the control of autonomous vehicles at the grip limit [11], [12], and even performance analysis of race motorcycles [13].

The second research field covers minimum-lap-time vehicle dynamics. The most common approaches are quasi-steady-state or transient lap time simulations [14], [15]. In quasi-steady-state methods, the path on the circuit is given and subdivided into sections of constant curvature, where the maximum steady-state acceleration values are determined [7]. This can be done on the basis of a g-g diagram [16]. To study the transient behavior of a race car, more complex models are necessary which include, e.g., the yaw dynamics. The first proper foray into numerical lap time optimization with a transient vehicle model came with [17], where the path and the velocity of a F1 car were jointly optimized using non-linear programming (NLP). The method was further extended in [18] with a more advanced tire model, and computational time was drastically improved by introducing curvilinear coordinates and numerical modifications in [19], [20]. The problem was also solved for a go-kart [21]. A comparison of direct NLP methods and indirect methods is given in [22]. An alternative approach is to decouple the determination of the optimal path from the minimum time problem. In [23], a convex optimization framework was proposed, with the tire friction circle formulated as a second-order cone constraint. Recently, the focus was put on model predictive control approaches for the time-optimal online control of autonomous race cars. Some authors have applied convex optimization [24], [25], while others relied on NLP [26], [27]. In [28], iterative learning control was combined with a trajectory modification algorithm to gradually minimize the experimental lap time. All these approaches do not include the modeling and control of the powertrain.

The third stream of research deals with time-optimal energy management by only modeling the longitudinal vehicle dynamics. A fixed path is assumed and a maximum velocity profile is used to model the tire grip limits by constraining the velocity in the braking zones, corners and corner exits. The original formulation was in the form of a second-order cone program [29]. Extensions included gearshift optimization with an iterative scheme [30], the optimization of a continuously variably transmission [31], the consideration of thermal constraints stemming from the electric motors using a quasi-convex formulation [32] and the optimization of the low-level operation of the F1 powertrain with NLP [33]. The maximum velocity profile has several drawbacks: While it can be easily measured at points on the circuit where the car was actually grip-limited, extrapolation backwards in distance at corner entries and forwards at corner exits is required to specify a useful constraint, relying either on imprecise heuristics or on complex vehicle dynamic simulations. Moreover, scaling the maximum velocity profile to emulate different grip levels [34] is devoid of physical meaning, since in reality the car is not limited in velocity, but rather in the acceleration stemming from the total tire force.

Finally, some researchers have solved the minimum-lap-time energy management problem while also considering the lateral vehicle dynamics. This is mostly done with non-convex NLP, and whilst these methods use very precise transient models, they do not have optimality guarantees and are impractical for large parametric studies due to long computational times. For instance, the energy management, driving path and velocity profile of the F1 car were jointly optimized in [35]. For electric racing cars, the time-optimal interactions between the energy management and the driving path were investigated in [36], [37], and thermal constraints on the powertrain were considered in [38]. Similarly, an indirect method was applied to solve the minimum lap time problem for a series-hybrid car [39]. While researchers lately have proposed extremely fast-computing NLP

methods such as the alternating direction method of multipliers to solve the energy management problem of road cars [40], these were not yet adapted to the race car problem. Quite recently, convex optimization [41] was used with a tire friction circle to study the effect of torque vectoring in electric race cars on a fixed driving path.

B. Research Statement

To the best of the authors' knowledge, so far there exist no simple phenomenological models for the performance envelope of a race car that can be formulated as convex constraints, have a useful number of fitting parameters and can be easily identified with measurement data collected on the car. In this paper, we bridge the gap between the approaches relying on a maximum velocity profile and the fully transient models. We therefore focus on a computationally efficient optimization framework for the minimum lap time energy management problem which includes a performance envelope model and addresses some of the drawbacks of the maximum velocity profile approach. Such a tool can be used to investigate the effect of different tire grip levels on the energy management strategies, to conduct parameter studies, to generate reference trajectories for causal controllers and to benchmark them.

C. Contributions

Our contribution is threefold: First, we propose a set of second-order cone and linear (in-)equality constraints that limit the accelerations of the vehicle directly in the g-g diagram, assuming a fixed driving path. This formulation differs from other approaches such as [23], [41], which rather constrain the forces of the individual tires, and facilitates the identification of the model with data commonly recorded on race cars. We include a velocity dependency to account for race cars with aerodynamic downforce. To increase the degrees of freedom in terms of fitting parameters of the model, we split the longitudinal acceleration variable into a positive and negative part. As far as we know, our splitting technique is novel and has not been proposed yet for this type of problem. It enables us to constrain acceleration and braking differently. The resulting second-order cone program is solved with optimality guarantees. Second, we present a systematic parameter identification approach for this particular model, in the form of an auxiliary optimization problem. Thus, the performance envelope model can be directly identified in the g-g diagram based on measurement data. This differs from the methods found in literature, where the boundary of the feasible space in the g-g diagram is determined using simulations of the vehicle dynamics [10], [15], [16]. Third, we validate the entire approach by comparing the optimization results with measurement data. Additionally, a comparison between the obtained energy management strategies and those yielded by the state-of-the-art method [29] based on a maximum velocity profile shows that our vehicle dynamics model is sufficiently accurate for the purposes of energy management optimization.

D. Outline

The case study of a state-of-the-art hybrid-electric F1 race car serves to illustrate our approach. The remainder of the paper is structured as follows: In Section II, we formulate the minimum lap time problem and introduce the modeling equations for the performance envelope. We then describe the parameter identification procedure in Section III and showcase it with data of the F1 car. In Section IV, we discuss the numerical solution of the optimization problem and compare the results to the measurement data and to the solution obtained with the state-of-the-art method. Section V concludes the paper and gives an outlook on future research.

II. Modeling

In this section, we formulate a model for the vehicle dynamics performance envelope in the form of convex constraints. We first introduce the concept of lap time minimization and the necessary relaxations and reformulations which lead to a second-order cone program [29]. Some details on second-order cone programs are given in Appendix A. We then present the model of the drag forces, followed by the novel performance envelope model. Finally, we summarize the modeling equations for the hybrid-electric F1 power unit as introduced in [29] and state the optimal control problem. The identification of the model parameters is discussed separately in Section III. All the measurements shown in the subsequent sections were recorded by means of telemetry on a state-of-the-art F1 car during a complete dry lap of the Silverstone Grand Prix Circuit. For reasons of confidentiality, some data has been normalized.

A. Minimum Lap Time Optimization

To achieve convexity, our approach builds on the assumption that the path on the track, parameterized by the independent path variable $s \in [0, S]$, is known a priori and not subject to optimization. Hence we assume that the path curvature $\gamma(s)$ is also known. It is related to the corner radius $r(s)$ by

$$\gamma(s) = \frac{1}{r(s)}. \tag{1}$$

The vehicle path for minimum lap time is called the 'racing line' and in general differs strongly from the center line of the racetrack. In [17], several methods for obtaining the racing line are described. In practice, the vehicle path is solely determined by the driver and his steering input. For the case studies presented in this paper, the racing line in the form of $\gamma(s)$ was therefore synthesized from velocity and acceleration measurements of one representative lap driven by an expert driver.

The objective of the optimization problem is to minimize the lap time T along the racing line on a certain race circuit. Since the track data is distance-based, we write the problem in space domain and then apply relaxations and reformulations that render the problem convex. For a start, the objective can be manipulated as follows:

$$\min T = \min \int_0^T \mathrm{d}t = \min \int_0^S \frac{\mathrm{d}t}{\mathrm{d}s}(s) \cdot \mathrm{d}s, \tag{2}$$

making it linear in the term $\frac{\mathrm{d}t}{\mathrm{d}s}(s)$, which is called *lethargy* [29] and represents the time consumption per unit distance. It is related to the velocity v of the car by

$$\frac{\mathrm{d}t}{\mathrm{d}s}(s) = \frac{1}{v(s)}. \tag{3}$$

Equation (3) is the link between the lap time integration in (2) and the velocity of the race car. Both the lethargy and the velocity are independent optimization variables, making (3) a non-convex constraint. However, it can be relaxed to inequality, resulting in the geometric mean expression

$$\frac{\mathrm{d}t}{\mathrm{d}s}(s) \cdot v(s) \geq 1. \tag{4}$$

Using the technique described in [29], we rewrite this in the form of the second-order cone constraint

$$\frac{\mathrm{d}t}{\mathrm{d}s}(s) \cdot \tilde{v} + v(s) \cdot \frac{1}{\tilde{v}} \geq \left\| \begin{matrix} 2 \\ \frac{\mathrm{d}t}{\mathrm{d}s}(s) \cdot \tilde{v} - v(s) \cdot \frac{1}{\tilde{v}} \end{matrix} \right\|_2, \tag{5}$$

where $\tilde{v} = 1\,\mathrm{m/s}$ is a normalization constant. By the objective (2), it is optimal to minimize the lethargy, and thus (5) will hold with equality in the optimal solution, meaning that the originally intended constraint (3) will be fulfilled [29].

Next, we model the longitudinal dynamics of the car. We consider the race car as a point mass m moving with velocity v along the racing line. Its longitudinal dynamics are characterized by Newton's second law

$$a_{\mathrm{long}} = \frac{1}{m} \cdot \sum F_{\mathrm{long}}, \tag{6}$$

which relates the longitudinal acceleration a_{long} to the sum of the forces F_{long} acting in longitudinal direction. However, this cannot be implemented directly in a second-order cone program. Indeed, by applying the chain rule, we obtain

$$a_{\mathrm{long}} = \frac{\mathrm{d}v}{\mathrm{d}t} = \frac{\mathrm{d}s}{\mathrm{d}t} \cdot \frac{\mathrm{d}v}{\mathrm{d}s} = v \cdot \frac{\mathrm{d}v}{\mathrm{d}s}, \tag{7}$$

which is a non-convex expression. To circumvent this problem, we introduce the normalized kinetic energy of the car as

$$\tilde{E}_{\mathrm{kin}} = \frac{1}{2} \cdot v^2. \tag{8}$$

The spatial derivative of this quantity is equal to the longitudinal acceleration

$$\frac{\mathrm{d}}{\mathrm{d}s}\tilde{E}_{\mathrm{kin}} = v \cdot \frac{\mathrm{d}v}{\mathrm{d}s} = a_{\mathrm{long}}. \tag{9}$$

Hence, the longitudinal dynamics (7) can be written in a linear fashion as

$$\frac{\mathrm{d}}{\mathrm{d}s}\tilde{E}_{\mathrm{kin}}(s) = \frac{1}{m} \cdot (F_{\mathrm{p}}(s) - F_{\mathrm{d}}(s)), \tag{10}$$

where F_{p} is the propulsive force acting at the driven wheels, while F_{d} represents the external drag forces acting on the vehicle. These forces will be modeled in Section II-B. Since we optimize only a single lap, we add a periodicity constraint on the kinetic energy state variable

$$\tilde{E}_{\mathrm{kin}}(S) = \tilde{E}_{\mathrm{kin}}(0). \tag{11}$$

The only problem left to resolve is the non-convex equality constraint (8) linking the kinetic energy to the velocity and thus, by (5), to the objective. We relax it to the inequality

$$\tilde{E}_{\mathrm{kin}}(s) \geq \frac{1}{2} \cdot v(s)^2 \tag{12}$$

and then rewrite it as a second-order cone constraint:

$$2 \cdot \tilde{E}_{\mathrm{kin}}(s) \cdot \frac{1}{\tilde{v}^2} + 1 \geq \left\| \begin{matrix} 2 \cdot v(s) \cdot \frac{1}{\tilde{v}} \\ 2 \cdot \tilde{E}_{\mathrm{kin}}(s) \cdot \frac{1}{\tilde{v}^2} - 1 \end{matrix} \right\|_2. \tag{13}$$

The following reasoning supports the claim that this relaxation is admissible: In order to minimize the lethargy, the velocity must be maximized, as is apparent in (4). Hence, (13) will hold with equality in the optimal solution, meaning that the physical relationship (8) will be respected.

B. Propulsive and Drag Forces

P_{u} denotes the total power produced by the race car's power unit and delivered at the driven wheels. Not all of this power propels the vehicle; some of it is lost in wheel slip [29]. We use a linear wheel slip equation to model these losses. The propulsive power is then

$$P_{\mathrm{p}}(s) = c_{\mathrm{s}} \cdot P_{\mathrm{u}}(s) - P_{\mathrm{brk}}(s), \tag{14}$$

where c_{s} is the wheel slip coefficient subject to identification, and $P_{\mathrm{brk}} \geq 0$ is the power dissipated in the friction brakes. Using the fact that force and power are linked by

$$F(s) = \frac{P(s)}{v(s)} = P(s) \cdot \frac{\mathrm{d}t}{\mathrm{d}s}(s), \tag{15}$$

we express (14) in terms of forces and obtain an equation for the propulsive force featuring in (10):

$$F_{\mathrm{p}}(s) = c_{\mathrm{s}} \cdot F_{\mathrm{u}}(s) - F_{\mathrm{brk}}. \tag{16}$$

The external drag forces acting on the vehicle are the aerodynamic drag F_{aero}, the hill force F_{grav} and the rolling friction F_{roll}:

$$F_{\mathrm{d}}(s) = F_{\mathrm{aero}}(s) + F_{\mathrm{grav}}(s) + F_{\mathrm{roll}}(s). \tag{17}$$

The aerodynamic drag force is assumed to be proportional to the velocity squared. Additionally, we include a term that depends on the path curvature $\gamma(s)$ of the racing line. This is useful when dealing with open-wheel race cars [29]. The modeling equation is then

$$F_{\mathrm{aero}}(s) = (c_{\mathrm{d},0} + c_{\mathrm{d},1} \cdot \gamma(s)) \cdot v(s)^2, \tag{18}$$

where $c_{\mathrm{d},0}$ and $c_{\mathrm{d},1}$ are parameters that have to be identified with measurement data. For the inclusion in the second-order cone program, this equation has to be linearized using the kinetic energy variable, resulting in

$$F_{\mathrm{aero}}(s) = (c_{\mathrm{d},0} + c_{\mathrm{d},1} \cdot \gamma(s)) \cdot 2 \cdot \tilde{E}_{\mathrm{kin}}(s). \tag{19}$$

Denoting by $g = 9.81\,\mathrm{m/s^2}$ the gravitational constant, the hill force depends on the track's slope $\theta(s)$ as

$$F_{\mathrm{grav}}(s) = m \cdot g \cdot \sin(\theta(s)). \tag{20}$$

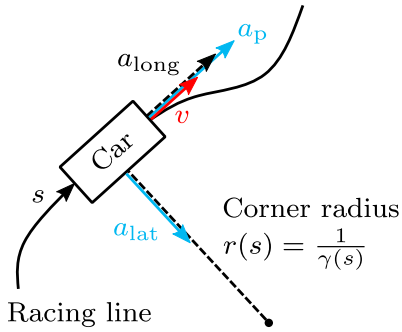

Fig. 3. The vehicle dynamics model assumes a quasi-steady-state condition of motion, separating the acceleration in longitudinal and lateral components. For the depicted case, the vehicle is accelerating. Usually, the effective longitudinal acceleration a_{long} is smaller in magnitude than the propulsive acceleration proportional to the propulsive force $a_{\mathrm{p}} \propto F_{\mathrm{p}}$, due to the drag forces acting on the car (except for steep hill descents).

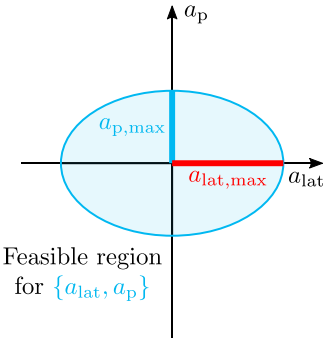

Fig. 4. Schematic representation of an elliptic bound in the g-g diagram, given by (26). The half-axes of the ellipse are denoted by $a_{\mathrm{lat,max}}$ and $a_{\mathrm{p,max}}$.

Finally, the rolling friction is characterized by

$$F_{\mathrm{roll}}(s) = c_{\mathrm{roll}} \cdot m \cdot g \cdot \cos(\theta(s)), \tag{21}$$

with the parameter c_{roll} subject to identification.

C. Performance Envelope Model

So far, for this type of convex energy management problems, the grip limit of the race car was modeled with a position-dependent maximum velocity profile v_{max} by imposing the following constraint on the normalized kinetic energy:

$$\tilde{E}_{\mathrm{kin}}(s) \leq \frac{1}{2} \cdot v_{\mathrm{max}}^2(s). \tag{22}$$

By contrast, in this section, we formulate a set of convex constraints that model the performance envelope of the race car. It limits the achievable longitudinal acceleration and deceleration as a function of the lateral acceleration by specifying a feasible set in the g-g diagram. Ultimately, it is comparable to a quasi-steady-state approach: The longitudinal dynamics are taken explicitly into account, as described in Section II-A, while the lateral dynamics are not modeled. We start by defining two auxiliary optimization variables, as illustrated in Fig. 3.

The first one is the component a_{p} of the longitudinal acceleration that is proportional to the propulsive force:

$$a_{\mathrm{p}}(s) = \frac{1}{m} \cdot F_{\mathrm{p}}(s). \tag{23}$$

The second one is the lateral acceleration a_{lat}. In a quasi-steady-state approximation [17], it increases with the square of the velocity and is inversely proportional to the cornering radius, resulting in the well-known formula derived from uniform circular motion [7]:

$$a_{\mathrm{lat}}(s) = \frac{v(s)^2}{r(s)} = v(s)^2 \cdot \gamma(s). \tag{24}$$

This equality constraint can be linearized by substituting the normalized kinetic energy

$$a_{\mathrm{lat}}(s) = 2 \cdot \tilde{E}_{\mathrm{kin}}(s) \cdot \gamma(s). \tag{25}$$

We now derive a set of elliptic boundary constraints that models the feasible $\{a_{\mathrm{lat}}(s), a_{\mathrm{p}}(s)\}$ in a g-g diagram. Indeed, the set enclosed by an ellipse is convex [42]. Our phenomenological model is instigated by two reasons: First, the boundaries of g-g diagrams depicted in literature [7] and in Fig. 1 bear resemblance to an ellipse. Second, the model is akin to Kamm's friction circle, which is often used in literature to describe the capability of an individual tire to transmit forces in longitudinal and lateral direction [43], but applied to the whole vehicle. The proposed boundary thus captures the limitations imposed by the achievable combined friction force of all four tires. Regarding the component in the longitudinal direction, the constraint is put on a_{p} rather than a_{long}. Indeed, a_{p} is proportional to the forces transmitted by the tires, whilst a_{long} includes the effect of the external forces, such as aerodynamic drag, and powertrain limitations. In our model, these effects will be superimposed as additional constraints. In its simplest form, an elliptic boundary in the g-g diagram is parameterized by the length of its half-axes $a_{\mathrm{p,max}} > 0$ and $a_{\mathrm{lat,max}} > 0$, as shown in Fig. 4. Through a series of simple manipulations, it can be stated equivalently as a second-order cone constraint:

$$\frac{a_{\mathrm{p}}(s)^2}{a_{\mathrm{p,max}}^2} + \frac{a_{\mathrm{lat}}(s)^2}{a_{\mathrm{lat,max}}^2} \leq 1 \tag{26}$$

$$\Leftrightarrow \quad a_{\mathrm{p}}(s)^2 + \left(\frac{a_{\mathrm{p,max}}}{a_{\mathrm{lat,max}}} \cdot a_{\mathrm{lat}}(s) \right)^2 \leq a_{\mathrm{p,max}}^2 \tag{27}$$

$$\Leftrightarrow \quad \left\| \begin{matrix} a_{\mathrm{p}}(s) \\ \frac{a_{\mathrm{p,max}}}{a_{\mathrm{lat,max}}} \cdot a_{\mathrm{lat}}(s) \end{matrix} \right\|_2 \leq a_{\mathrm{p,max}}. \tag{28}$$

Next, we extend (28) to capture two relevant effects. First, the exploitable grip limit during braking and acceleration might be different, and in practice it is more difficult for a driver to fully exploit the combined braking/cornering capabilities compared to combined acceleration/cornering [7]. Hence, we implement a different elliptic boundary for acceleration ($a_{\mathrm{p}} \geq 0$) and deceleration phases ($a_{\mathrm{p}} < 0$), as depicted schematically in Fig. 5. This increases the degrees of freedom when fitting the performance envelope model to measurement data. Since the second-order cone formulation (28) of an elliptic constraint describes an entire ellipse, a positive and a negative acceleration component a_{p}^+ and a_{p}^- have to be introduced in order to constrain acceleration and

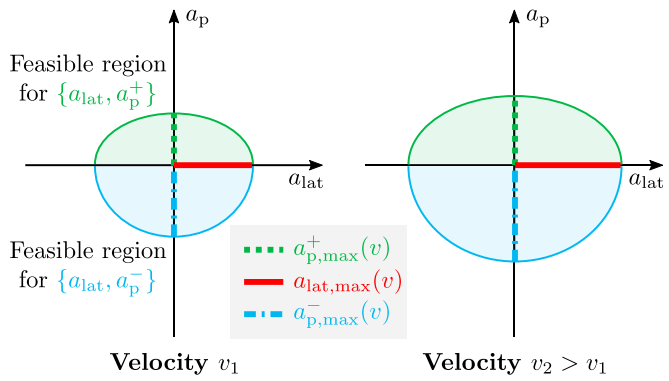

Fig. 5. Schematic representation of the proposed performance envelope model. As velocity increases, the half-axes that define the upper and lower half-ellipses are scaled homogeneously according to (34), (36), (37).

deceleration differently. These variables are limited by

$$a_\mathrm{p}^+(s) \geq 0, \tag{29}$$

$$a_\mathrm{p}^-(s) \leq 0, \tag{30}$$

and their sum must correspond to the actual propulsive acceleration:

$$a_\mathrm{p}(s) = a_\mathrm{p}^+(s) + a_\mathrm{p}^-(s). \tag{31}$$

We then constrain the positive component by

$$\left\| \begin{matrix} a_\mathrm{p}^+(s) \\ \frac{a_\mathrm{p,max}^+}{a_\mathrm{lat,max}} \cdot a_\mathrm{lat}(s) \end{matrix} \right\|_2 \leq a_\mathrm{p,max}^+ \tag{32}$$

linking a_p^+ and a_lat, and analogously the negative component is subject to

$$\left\| \begin{matrix} a_\mathrm{p}^-(s) \\ \frac{a_\mathrm{p,max}^-}{a_\mathrm{lat,max}} \cdot a_\mathrm{lat}(s) \end{matrix} \right\|_2 \leq a_\mathrm{p,max}^- \tag{33}$$

linking a_p^- and a_lat. As indicated in Fig. 5, the parameters $a_\mathrm{lat,max}$, $a_\mathrm{p,max}^+$ and $a_\mathrm{lat,max}$, $a_\mathrm{p,max}^-$ denote the half-axes of the upper and lower half-ellipses, respectively. The half-axis $a_\mathrm{lat,max}$ must have an identical value for both ellipses, to avoid a discontinuity under pure lateral acceleration. The validity of the proposed 'split acceleration' approach will be verified and explained when analyzing the optimization results in Section IV-C.

Second, we include a velocity dependency into our performance envelope model in order to account for the effect of aerodynamic downforce. This phenomenon is clearly visible in the measurement data in Fig. 1, where the achieved lateral acceleration is significantly higher at high velocity. As described in [7], the downforce generated by the aero devices is approximately proportional to the velocity squared, hence the normal force on the tires increases at the same rate, leading to limits on longitudinal and lateral acceleration that increase with velocity. Consequently, we model the maximum lateral acceleration (i.e., the horizontal half-axis of the half-ellipses in Fig. 5) as a quadratic function of velocity:

$$a_\mathrm{lat,max}(v(s)) = c_1 \cdot v(s)^2 + c_2 \cdot v(s) + c_3, \tag{34}$$

with the fitting parameters c_1, c_2 and c_3. We then formulate an equivalent linear version of this constraint by substituting the kinetic energy variable, leading to

$$a_\mathrm{lat,max}(s) = 2 \cdot c_1 \cdot \tilde{E}_\mathrm{kin}(s) + c_2 \cdot v(s) + c_3. \tag{35}$$

The acceleration and deceleration capabilities of the vehicle in longitudinal direction also increase with velocity. However, to preserve convexity, the ratios $a_\mathrm{p,max}^+/a_\mathrm{lat}$ and $a_\mathrm{p,max}^-/a_\mathrm{lat}$ in (32) and (33) must not be a function of any optimization variable, and more specifically, must not be a function of the velocity or the kinetic energy variable. We thus set these ratios to the constant fitting parameters $r^+ > 0$ and $r^- > 0$ defined as

$$r^+ = \frac{a_\mathrm{p,max}^+(s)}{a_\mathrm{lat,max}(s)}, \tag{36}$$

$$r^- = \frac{a_\mathrm{p,max}^-(s)}{a_\mathrm{lat,max}(s)}. \tag{37}$$

Hence, the feasible region in the g-g diagram changes in a shape-preserving manner as a function of velocity, as shown schematically in Fig. 5. This convexity requirement reduces the degrees of freedom when fitting the g-g diagram boundary, since rather than identifying individual quadratic functions of v for $a_\mathrm{p,max}^+$ and $a_\mathrm{p,max}^-$, these quantities are linked to the velocity dependency of $a_\mathrm{lat,max}$. Nonetheless, we will show in Section IV that measurement data can be reproduced with very satisfying precision using the presented approach.

By inserting (35), (36) in (32) and (35), (37) in (33), respectively, we obtain the second-order cone constraints

$$\left\| \begin{matrix} a_\mathrm{p}^+(s) \\ r^+ \cdot a_\mathrm{lat}(s) \end{matrix} \right\|_2 \leq r^+ \cdot \left(2 \cdot c_1 \cdot \tilde{E}_\mathrm{kin}(s) + c_2 \cdot v(s) + c_3 \right), \tag{38}$$

$$\left\| \begin{matrix} a_\mathrm{p}^-(s) \\ r^- \cdot a_\mathrm{lat}(s) \end{matrix} \right\|_2 \leq r^- \cdot \left(2 \cdot c_1 \cdot \tilde{E}_\mathrm{kin}(s) + c_2 \cdot v(s) + c_3 \right). \tag{39}$$

To summarize, the model (38), (39) for the boundary of the performance envelope consists of two velocity-dependent half-ellipses in the g-g diagram. It is fully described by the five constant parameters $\{c_1, c_2, c_3, r^+, r^-\}$. The parameter identification procedure will be discussed in Section III.

D. Powertrain Model

To complete the lap time optimization problem, we have to formulate the equations that model the powertrain [29]. In the simplest form, such a model could consist of linear inequality constraints of the form

$$P_\mathrm{u,min} \cdot \frac{\mathrm{d}t}{\mathrm{d}s}(s) \leq F_\mathrm{u}(s) \leq P_\mathrm{u,max} \cdot \frac{\mathrm{d}t}{\mathrm{d}s}(s), \tag{40}$$

where the parameters $P_\mathrm{u,min}$ and $P_\mathrm{u,max}$ limit the power that is achievable by the race car's power unit.

For the energy management of a Formula 1 car under the current technical regulations, the power flows shown in Fig. 6 must be considered. Denoting by P_e the engine power and by

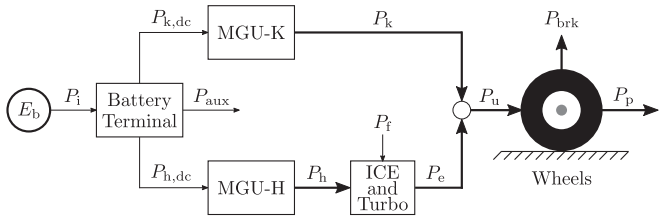

Fig. 6. Schematic representation of the power flows in the F1 powertrain. Thick arrows illustrate mechanical power, whilst thin arrows illustrate electrical power (with the exception of the chemical fuel power).

P_{k} the power of the MGU-K, the total power delivered by the power unit to the driven rear wheels is given by

$$P_{\mathrm{u}}(s) = P_{\mathrm{e}}(s) + P_{\mathrm{k}}(s). \tag{41}$$

Using (15), we obtain for the power unit force:

$$F_{\mathrm{u}}(s) = F_{\mathrm{e}}(s) + F_{\mathrm{k}}(s). \tag{42}$$

The fuel mass flow $\dot{m}_{\mathrm{f}}$ with lower heating value H_{lhv} defines the fuel power

$$P_{\mathrm{f}}(s) = H_{\mathrm{lhv}} \cdot \dot{m}_{\mathrm{f}}, \tag{43}$$

which is constrained by the technical regulations [4] to

$$P_{\mathrm{f}}(s) \leq H_{\mathrm{lhv}} \cdot \dot{m}_{\mathrm{f,max}}. \tag{44}$$

For the purposes of a high-level energy management optimization, the engine power can then be quantified with the simple Willans model [29]

$$P_{\mathrm{e}}(s) = \eta_{\mathrm{e}} \cdot P_{\mathrm{f}}(s) - P_{\mathrm{e},0}, \tag{45}$$

where η_{e} denotes the Willans efficiency and $P_{\mathrm{e},0}$ the engine drag power. Moreover, the MGU-H can be assumed to operate only in generator mode, and its power is then related to the fuel power by the recuperation efficiency η_{h} as

$$P_{\mathrm{h}}(s) = \eta_{\mathrm{h}} \cdot P_{\mathrm{f}}(s). \tag{46}$$

Again using (15), the power variables in equations (44), (45), (46) are transformed into forces, leading to constraints that can be implemented in the second-order cone program:

$$F_{\mathrm{f}}(s) \geq 0, \tag{47}$$

$$F_{\mathrm{f}}(s) \leq H_{\mathrm{lhv}} \cdot \dot{m}_{\mathrm{f,max}} \cdot \frac{\mathrm{d}t}{\mathrm{d}s}(s), \tag{48}$$

$$F_{\mathrm{e}}(s) = \eta_{\mathrm{e}} \cdot F_{\mathrm{f}}(s) - P_{\mathrm{e},0} \cdot \frac{\mathrm{d}t}{\mathrm{d}s}(s), \tag{49}$$

$$F_{\mathrm{h}}(s) = \eta_{\mathrm{h}} \cdot F_{\mathrm{f}}(s). \tag{50}$$

Next, the electrical components must be modeled. The power drawn from or fed to the battery terminals is given by

$$P_{\mathrm{b}}(s) = P_{\mathrm{k,dc}}(s) + P_{\mathrm{h,dc}}(s) + P_{\mathrm{aux}}, \tag{51}$$

where $P_{\mathrm{k,dc}}$ and $P_{\mathrm{h,dc}}$ denote the electrical power of the MGU-K and MGU-H, and P_{aux} models a small constant auxiliary power. Applying (15), this results in

$$F_{\mathrm{b}}(s) = F_{\mathrm{k,dc}}(s) + F_{\mathrm{h,dc}}(s) + P_{\mathrm{aux}} \cdot \frac{\mathrm{d}t}{\mathrm{d}s}(s). \tag{52}$$

It was shown in [29] that the electrical losses of the MGUs can be accurately modeled by the quadratic relationships

$$P_{\mathrm{k,dc}}(s) = \alpha_{\mathrm{k}} \cdot P_{\mathrm{k}}(s)^2 + P_{\mathrm{k}}(s), \quad \alpha_{\mathrm{k}} > 0, \tag{53}$$

$$P_{\mathrm{h,dc}}(s) = \alpha_{\mathrm{h}} \cdot P_{\mathrm{h}}(s)^2 + P_{\mathrm{h}}(s), \quad \alpha_{\mathrm{h}} > 0, \tag{54}$$

with α_{k} and α_{h} being the model parameters subject to identification. Similarly, the battery losses are captured with the internal battery power P_{i} given by

$$P_{\mathrm{i}}(s) = \alpha_{\mathrm{b}} \cdot P_{\mathrm{b}}(s)^2 + P_{\mathrm{b}}(s), \quad \alpha_{\mathrm{b}} > 0, \tag{55}$$

with the model parameter α_{b}. The relationships (53), (54), (55) are of the form

$$P_{\mathrm{y}}(s) = \alpha \cdot P_{\mathrm{x}}(s)^2 + P_{\mathrm{x}}(s), \quad \alpha > 0. \tag{56}$$

Following a loss-less relaxation reasoning [44], this is relaxed to the convex inequality constraint

$$P_{\mathrm{y}}(s) \geq \alpha \cdot P_{\mathrm{x}}(s)^2 + P_{\mathrm{x}}(s), \quad \alpha > 0, \tag{57}$$

which will hold with equality in the optimal solution. After applying (15), the inequality can be reformulated to the second-order cone constraint

$$\left\| \begin{matrix} 2 \cdot \sqrt{\alpha} \cdot F_{\mathrm{x}}(s) \cdot \frac{\tilde{v}}{\tilde{F}} \\ \frac{\mathrm{d}t}{\mathrm{d}s} \cdot \tilde{v} - (F_{\mathrm{y}} - F_{\mathrm{x}}) \cdot \frac{1}{\tilde{F}} \end{matrix} \right\|_2 \leq \frac{\mathrm{d}t}{\mathrm{d}s} \cdot \tilde{v} + (F_{\mathrm{y}} - F_{\mathrm{x}}) \cdot \frac{1}{\tilde{F}}, \tag{58}$$

where $\tilde{F} = 1\,\mathrm{N}$ is a normalization constant. For the sake of brevity, we do not discuss the reformulation in detail here, but refer to [29].

Finally, the relevant on-board energy reservoirs must be modeled. While the fuel force F_{f} is a purely mathematical concept, it allows to capture the evolution of the fuel energy consumption E_{f} in terms of its spatial derivative

$$\frac{\mathrm{d}}{\mathrm{d}s} E_{\mathrm{f}}(s) = F_{\mathrm{f}}(s), \tag{59}$$

while the battery energy varies as a function of the internal battery power, which in space domain translates to the corresponding force

$$\frac{\mathrm{d}}{\mathrm{d}s} E_{\mathrm{b}}(s) = -F_{\mathrm{i}}(s), \tag{60}$$

where the minus sign indicates that a positive power discharges the battery. To render the energy management problem well-posed, we specify initial and terminal conditions on the energy variables. For the fuel consumption integration, these are

$$E_{\mathrm{f}}(0) = 0, \quad E_{\mathrm{f}}(S) \leq E_{\mathrm{f,target}}, \tag{61}$$

and for the battery energy, we require

$$E_{\mathrm{b}}(0) = E_{\mathrm{b,init}}, \quad E_{\mathrm{b}}(S) \geq E_{\mathrm{b,init}} + \Delta E_{\mathrm{b,target}}, \tag{62}$$

where $E_{\mathrm{b,init}}$ denotes the initial battery energy content. The energy consumption is thus constrained by the strategy-defined parameters $E_{\mathrm{f,target}}$ and $\Delta E_{\mathrm{b,target}}$. The F1 regulations [4] specify additional limits on the allowed boosting and recuperation per lap, which are implemented in the model but not discussed here. For the modeling of those quantities, interested readers are again referred to [29].

E. Minimum Lap Time Control Problem

For the F1 powertrain, the minimimum lap time control problem is then formulated as follows:

***Problem 1**:* With the performance envelope, the energy management strategies for minimum lap time are the solution of

$$\min \int_0^S \frac{\mathrm{d}t}{\mathrm{d}s}(s) \cdot \mathrm{d}s$$

subject to the constraints

Kinematics:	(5), (10), (11), (13),
Propulsive and drag forces:	(16), (17), (19), (20), (21),
Performance envelope:	(23), (25), (29), (30),
	(31), (38), (39),
Powertrain (F1):	(47), (48), (49), (50), (52),
	(58), (59), (60), (61), (62).

This convex optimization framework is flexible in the sense that for a race car with a powertrain layout differing from the F1 power unit, it is sufficient to modify the constraints related to the powertrain and to adapt the model parameters.

III. Parameter Identification

To showcase the proposed optimization framework, we will solve Problem 1 for a current-generation hybrid-electric F1 race car. The model parameters pertaining to the drag forces and the powertrain (see Sections II-B and II-D) were already identified and validated in [29]. Hence, we do not discuss the parameter identification for these components here.

We focus on the parameters $\{c_1, c_2, c_3, r^+, r^-\}$ that describe the convex performance envelope presented in Section II-C. Whilst it is possible to determine the boundary of the feasible space in the g-g diagram by means of simulation [15], [16], our approach works directly with measurement data. We assume that the given data set consists of N data points d_i comprising acceleration and velocity values and the throttle pedal position u_{th}:

$$d_i = \{a_{\mathrm{lat},i}, a_{\mathrm{p},i}, v_i, u_{\mathrm{th},i}\} \quad \text{for} \quad i = 1, \ldots, \mathrm{N}. \tag{63}$$

The proposed performance envelope represents a boundary that models the feasible region for $\{a_{\mathrm{lat}}, a_{\mathrm{p}}\}$ in the g-g diagram. To be robust against outliers, we do not determine the smallest envelope that encloses all the data points, but we rather seek the velocity-dependent half-ellipses that best represent the varying boundary in the g-g diagram. Therefore, we have to extract the data points that correspond to a *grip-limited* operation of the car. We assume that in the quest to minimize lap time, an expert race driver is demanding full power from the powertrain whenever possible, that is, whenever the driver is not constrained by the grip limit of the tires. Consequently, for classification we use the throttle pedal signal to determine whether a data point belongs to the grip-limited set GL, according to the following rule:

$$u_{\mathrm{th},i} < 100\,\% \quad \rightarrow \quad i \in GL \quad \text{for} \quad i = 1, \ldots, \mathrm{N}. \tag{64}$$

For our case study, we use telemetry data from a state-of-the-art F1 car, collected with a sampling time of 0.01 s on the Silverstone Circuit. Fig. 7 shows the grip-limited data points in g-g diagrams for different velocity categories, where v_0 denotes a normalization constant. Generally, the velocity of a F1 car varies between roughly 15 m/s in the slowest corners and 100 m/s on the longest straights.

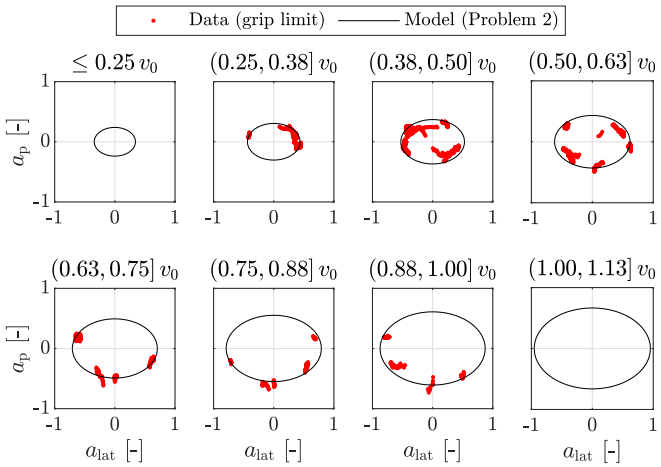

Fig. 7. Representation of the data points classified as grip-limited according to (64), together with the performance envelope model identified by solving Problem 2. In each plot, the two half-ellipses (38), (39) obtained for the upper bound of the corresponding velocity category are plotted, along with the data points falling in that category. There are no data points for the categories with lowest and highest velocity. These ellipses are just shown to illustrate the speed-dependency of the model. The velocity categories were normalized with the same nominal velocity v_0 as the horizontal axis in Fig. 8.

Three comments are in order: First, as expected, the points lie further away from the origin as velocity increases, due to the aerodynamic downforce. Second, while most points indeed seem to form some sort of boundary of the g-g diagram space, a few lie towards the inside of the others. This is visible in the categories $(0.38, 0.50]\,v_0$ and $(0.50, 0.63]\,v_0$. These points are stemming from fast transitions, for instance from right-hand to left-hand corners, where due to the vehicle's yaw, roll and pitch dynamics, the driver was neither able to operate the vehicle at the grip limit of the tires, nor to request full power. It is not a trivial task to eliminate these points in an automated fashion from the data set, which is why we simply include them in the fitting procedure. Third, the number of data points in each velocity category naturally depends on the characteristics of the racetrack, i.e., the number of slow, medium-speed and fast corners. With these preparations, we propose the following parameter identification procedure:

***Problem 2**:* The parameters that characterize the performance envelope of a given race car on a given circuit are the solution to the following optimization problem:

$$\min_{c_1, c_2, c_3, r^+, r^-} \quad \sum_{i \in GL} \delta_i(d_i, c_1, c_2, c_3, r^+, r^-),$$

where δ_i represents the distance between the data point d_i and the closest point on the performance envelope boundary model (i.e., the upper and lower half-ellipses) evaluated at the velocity v_i. Hence, δ_i is determined as follows:

if $a_{\mathrm{p},i} \geq 0$

$$\delta_i = \min_{\varphi\in[0,\pi]} \Bigg(\left(a_{\mathrm{p},i} - r^+ \cdot a_{\mathrm{lat,max}}(c_1,c_2,c_3,v_i)\cdot\sin(\varphi)\right)^2 + \left(a_{\mathrm{lat},i} - a_{\mathrm{lat,max}}(c_1,c_2,c_3,v_i)\cdot\cos(\varphi)\right)^2 \Bigg)^{1/2},$$

else

$$\delta_i = \min_{\varphi\in[-\pi,0]} \Bigg(\left(a_{\mathrm{p},i} - r^- \cdot a_{\mathrm{lat,max}}(c_1,c_2,c_3,v_i)\cdot\sin(\varphi)\right)^2 + \left(a_{\mathrm{lat},i} - a_{\mathrm{lat,max}}(c_1,c_2,c_3,v_i)\cdot\cos(\varphi)\right)^2 \Bigg)^{1/2}.$$

This case distinction ensures that the correct half-ellipse is considered for each data point.

In the objective of Problem 2, each data point has the same weight. For a given race track, the velocity range in which the car spends most time at the grip limit is thus best represented and has the largest impact on the objective. This is desirable in order to achieve a high lap time accuracy when using the identified performance envelope model in Problem 1. We solve Problem 2 with the *fminsearch* optimization routine provided by MATLAB, using reasonable initial guesses for the parameters. The resulting fit is shown in Fig. 7. Some data points lie outside of the largest ellipse for the respective velocity category, which means that they are not contained by the identified performance envelope. This is due to the nature of the objective defined in Problem 2: The goal is to find the envelope which best approximates the grip-limited data points in an 'average' sense, i.e., which minimizes the sum of the distances δ_i between the ellipses and the data points. An underestimation of a data point's grip level is penalized identically to an overestimation in the objective. Hence, the fitting method does not guarantee that all the data points lie inside the performance envelope, but overall it approximates the data in a suitable manner. In this particular case, there is only a very slight difference between the shapes of the upper and lower half-ellipses, i.e., the identified values of r^+ and r^- are very similar. The 'inflation' of the performance envelope with increasing velocity clearly reflects the effect of aerodynamic downforce.

The obtained velocity dependency of the model is also visualized in Fig. 8 by plotting the length of the ellipses' half-axes $a_{\mathrm{lat,max}}$, $a^+_{\mathrm{p,max}}$ and $a^-_{\mathrm{p,max}}$ as a function of velocity, together with all the measured data points. The horizontal axis of the figure has been normalized with respect to v_0. The identified $a_{\mathrm{lat,max}}$ from (34) is catching the achievable maximum lateral acceleration very nicely. We note that the dependency on the velocity is clearly less than quadratic, but rather almost linear, resulting in a very small identified value for c_1. Nonetheless, we keep the quadratic term to showcase the flexibility of the approach, since the additional degree of freedom might improve the precision in other applications. The effect of the almost linear velocity dependency was also observed and discussed in [7] and could be attributed to the load sensitivity of the tire friction coefficient. Indeed, the latter can decrease quite substantially with increasing tire load, which counteracts the effect of the

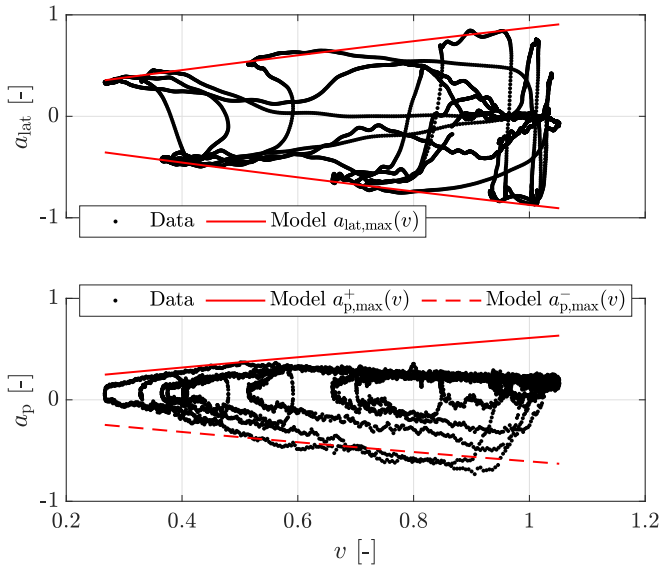

Fig. 8. Acceleration of a F1 car as a function of velocity, plotted together with the length of the half-axes of the half-ellipses describing the performance envelope. The latter are given by (34), (36), (37) and were identified by solving Problem 2. The effect of aerodynamic downforce is clearly visible, as the acceleration capability provided by the chassis and the tires increases with velocity. Section III gives a detailed discussion. The horizontal axis has been normalized with the constant v_0 also used in Fig. 7.

increasing normal force on the tire. Regarding the maximum longitudinal acceleration, we observe that the data points show a decreasing tendency for $v > 0.5\,v_0$. These data points are effectively power-limited, in the sense that the maximum acceleration which can be provided by the power unit is smaller than what the tires could potentially transmit. At $v < 0.5\,v_0$, where the grip limit of the tires actually determines the achievable acceleration, the identified $a^+_{\mathrm{p,max}}$ obtained from (36) captures the trend of the data. Since F1 cars have very powerful brakes, the power limit effect is not observed under deceleration, and $a^-_{\mathrm{p,max}}$ obtained from (37) is close to the boundary of the data points also at high velocity. Conversely, for $v < 0.5\,v_0$, there is a gap between $a^-_{\mathrm{p,max}}$ and the data points. This can be explained by the fact that at these speeds, the data points feature combined braking and cornering. Thereby, the driver starts turning into the corners while still pressing the brake pedal, a driving technique that is commonly referred to as trail-braking [45]. Our explanation is corroborated by Fig. 7, where for $v < 0.5\,v_0$ there are no data points with pure longitudinal deceleration (i.e., with $a_{\mathrm{p}} < 0$ and $a_{\mathrm{lat}} = 0$). Hence, the measured a_{p} does not reach the values that would be possible under pure longitudinal deceleration, which is what the half-axis of the ellipse describes. To a lesser extent, the equivalent effect of combined cornering and acceleration is observed for $v < 0.4\,v_0$ in Fig. 8.

Given the above considerations, defining an error criterion to quantify the quality of the fit with respect to the acceleration values makes little sense. Moreover, stating the value of the objective of Problem 2 by itself does not yield additional insights. We therefore choose to discuss the accuracy in terms of lap time and velocity profile when solving Problem 1 with the identified performance envelope.

IV. Results

In this section, we present the results obtained by solving the minimum lap time problem with the performance envelope model. To this end, Problem 1 is discretized using the standard Euler-forward method, resulting in a second-order cone program (see Appendix A for details). All the results shown were obtained with a spatial discretization step of $\Delta s = 5$ m. The implementation is done in MATLAB: The problem is parsed with YALMIP [46] and solved with the interior-point solver ECOS [47]. Since Problem 1 is convex, it can be solved with global optimality guarantees. Indeed, for the results presented in this section, the solver issued a certificate of optimality.

First, we discuss the velocity profile obtained as a result of the optimization. We compare it to measurement data, in order to validate the proposed performance envelope model. Second, we comment on the computational time required for solving the problem, as well as the choice of the discretization step. Third, we investigate in more detail the effect of the convex relaxations, the performance envelope constraints, and the split acceleration approach. Fourth, we analyze the energy management strategies and validate the approach by comparing them to the strategies generated with the state-of-the-art maximum velocity profile approach. Fifth, the effect of scaling the performance envelope is briefly analyzed. Sixth, we discuss the advantages of the performance envelope formulation, compared to the maximum velocity profile approach.

A. Optimal Solution and Vehicle Dynamics

In this section, we compare the optimization results with measurement data recorded by telemetry during a specific lap, in terms of velocity profile, lateral and longitudinal acceleration. In order to do so, the path curvature associated with the measurement has to be used in the constraints (19) and (25) when solving Problem 1. It can be obtained by post-processing the velocity and acceleration measurements following the method described in [17]. Right-hand corners are characterized by $\gamma < 0$, and left-hand corners by $\gamma > 0$.

First, we discuss the case of a lap of the Silverstone Circuit, for which we have already identified the parameters of the performance envelope in Section III. The track has a length of roughly 5900 m and can be lapped by a state-of-the-art F1 car in around 87 s. The results are shown in Fig. 9. The optimal velocity profile subject to the performance envelope and powertrain constraints is very similar to the measured one. In particular, the convex performance envelope constraints correctly capture the braking zones and corners. The difference in velocity Δv is contained between -3 and 3 m/s. This is similar to the level of precision achieved with quasi-steady-state simulations by other authors [10].

Under pure lateral acceleration, the model is very precise, underlined by the fact that at the apices of the corners (corresponding to local maxima or minima in the curvature γ), the difference in velocity is in general less than 1 m/s. One exception is the fast corner at $s \approx 3700$ m, where the achievable velocity is overestimated by around 2 m/s. Overall, the lateral acceleration therefore follows the measurement very closely. The results also

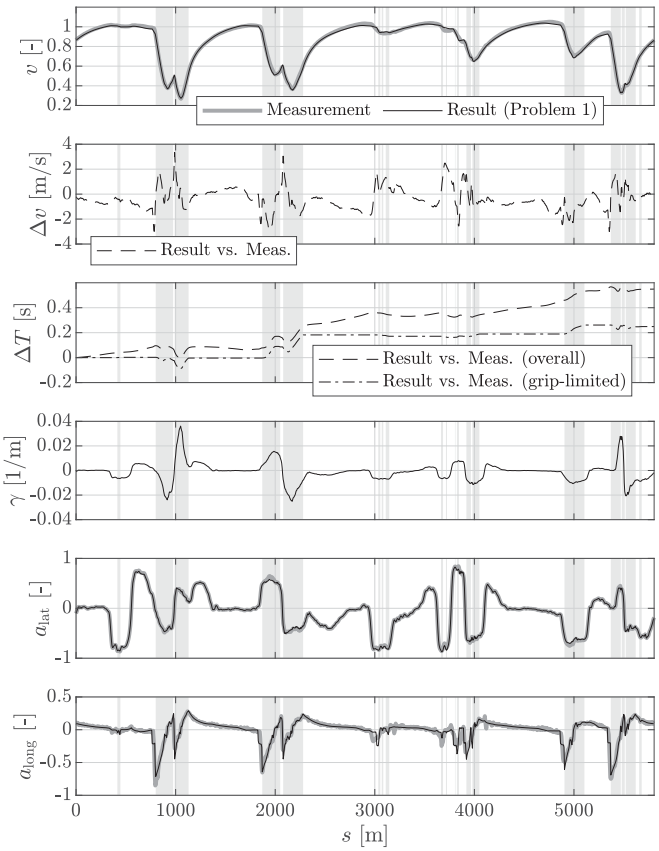

Fig. 9. **Silverstone Circuit:** Comparison between measurement data and the results obtained by solving Problem 1. Shaded in gray are the regions where it is optimal to operate the car at the limit of grip, i.e., where one of the performance envelope constraints (38), (39) holds with equality in the optimal solution of Problem 1. The signal Δv describes the velocity difference between the optimization result and the measurement data, whilst ΔT is the cumulative lap time difference.

signify that the modeled velocity dependency is sensible, as Silverstone is a circuit composed of high-speed corners, but also some slow turns. Such a track characteristic highlights the important aerodynamic downforce effect of a modern F1 car. The model captures all types of corners in a satisfying manner.

In the longitudinal acceleration, some differences are visible. In this particular case, the peak braking performance is a bit underestimated by the identified performance envelope, a feature which is already visible in Figs. 7 and 8 for high velocity. Moreover, on the straights some small differences appear due to the causal power unit energy management in the measurement, which differs slightly from the non-causal optimal solution of Problem 1. Velocity differences on the straight are not only due to the limitations of the performance envelope model, but also to the simple drag and power unit models used. As already discussed in [29], such a model is only a rough approximation, but nonetheless, the evolution of velocity on the straights is remarkably similar to the measurement.

Accordingly, the lap time difference ΔT is only 0.5 s. The cumulative time lost or gained when the grip limit constraints are active, i.e., the difference stemming directly from the performance envelope model, is even smaller and only amounts to

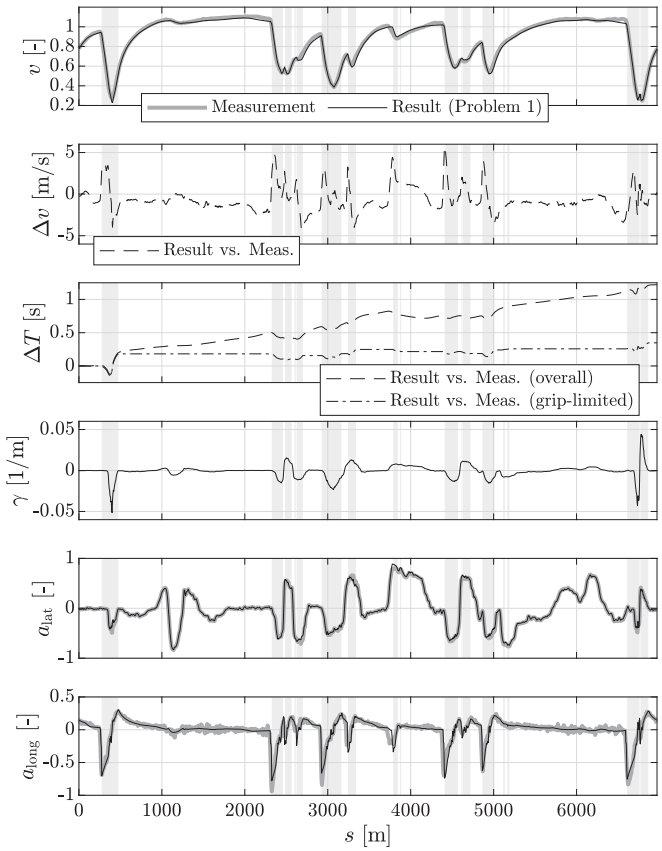

Fig. 10. **Spa-Francorchamps Circuit:** Comparison between measurement data and the results obtained by solving Problem 1. The plots are structured identically to the description given in Fig. 9.

0.25 s. This constitutes less than 0.3 % with respect to a typical lap time of the circuit in an F1 car.

In order to highlight that our method is applicable to different circuits and scenarios, Fig. 10 contains the results of a second case study conducted for a lap of the Spa-Francorchamps Circuit. This track has a length of roughly 7000 m and can be lapped by a F1 car in around 106 s. The parameters describing the performance envelope were re-identified for this particular circuit and scenario, due to the different configuration of the car and the different track grip levels. The velocity difference between our result and the measurement is generally observed to be within $\pm$ 4 m/s. The peak differences stem from slight mismatches in the braking points, which we will further comment on in Section IV-B. The cornering speeds are reproduced with a similar precision to the Silverstone case study, and this is also reflected by the lateral acceleration comparison. The long straights of this particular circuit exacerbate the effect of any imprecision in our drag and power unit model, leading to an overall lap time deviation of 1.2 s, a large part of which is accumulated between 500 m and 2200 m, and between 5000 m and 6500 m. However, the grip-limited regions only contribute 0.35 s to this value, again underlining the satisfactory precision of the proposed vehicle dynamics constraints.

To summarize, despite its simplicity, the performance envelope model can capture the limitations in the longitudinal and lateral dynamics of the car surprisingly well. The result is a highly satisfactory level of accuracy in terms of lap time.

TABLE I
COMPUTATIONAL TIME REQUIRED TO SOLVE PROBLEM 1

Discretization Δs	1 m	2 m	5 m	10 m
Comp. time for Silverstone	10.16 s	3.69 s	0.92 s	0.39 s
Comp. time for Spa	14.57 s	6.12 s	1.43 s	0.67 s

B. Computational Time and Discretization Step

Table I reports the computational time required to solve Problem 1 for different choices of the spatial discretization step Δs. The experiments were conducted on a standard consumer laptop with a 2.6 GHz processor and 16 GB RAM. As one would expect, the smaller Δs, the larger the number of optimization variables and the longer the computational time. Moreover, solving the problem for the Spa-Francorchamps Circuit generally takes longer than solving it for the Silverstone Circuit. This is due to the fact that the former track is longer, leading to more optimization variables after discretization. The computational times are in the order of 1 s to 10 s, highlighting the efficiency of the presented convex optimization approach. Moreover, they are almost identical to the ones reported in [29] for the state-of-the-art approach with a maximum velocity profile, indicating that the novel performance envelope constraints do not entail a penalty in computational time. They also compare favorably to the ones reported in [36] for a similar minimum-lap-time problem in the form of an NLP including path optimization, which were in the order of 1 min for $\Delta s = 5$ m on similar hardware.

Lastly, a comment on the choice of the discretization step is appropriate. The largest velocity differences in Figs. 9 and 10 occur at the beginning of the braking zones. Indeed, with a discretization step of 5 m, the measured braking point cannot always be captured accurately, even if the performance envelope models attained utmost precision. The braking point obtained in the solution will either be too early or too late, resulting in a large velocity difference due to the strong deceleration capability of a F1 car. Experiments with a discretization step of 1 m showed that this effect can be mitigated, albeit at the expense of computational time increasing by a factor of ten. However, the overall accuracy in terms of lap time did not improve significantly,[1] nor did the accuracy of the velocity profile in the corners and on the straights. We therefore deem a choice of $\Delta s = 5$ m a reasonable compromise between accuracy and computational time, especially if the optimization tool is to be used for parametric studies regarding the energy management.

C. Effect of the Performance Envelope Constraints

Fig. 11 shows that, as expected, the novel performance envelope model does not affect the relaxations that were necessary to obtain a convex formulation of the minimum lap time problem.

[1]In [29], with an identical Euler forward discretization method, it was also observed that accuracy does not improve significantly anymore for choices of Δs smaller than 10 m.

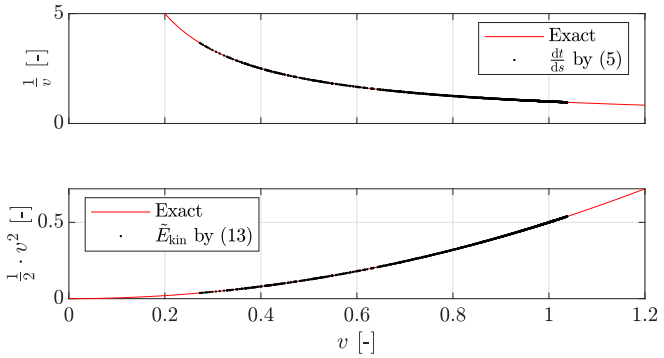

Fig. 11. Silverstone Circuit: The second-order cone constraints (5) and (13), linking $\frac{1}{v}$, $\frac{\mathrm{d}t}{\mathrm{d}s}$ and $\tilde{E}_{\mathrm{kin}}$, always hold with equality in the optimal solution of Problem 1. The lines in the plots show the exact relationship between these quantities according to (3) and (8), while the dots represent the data from the optimal solution.

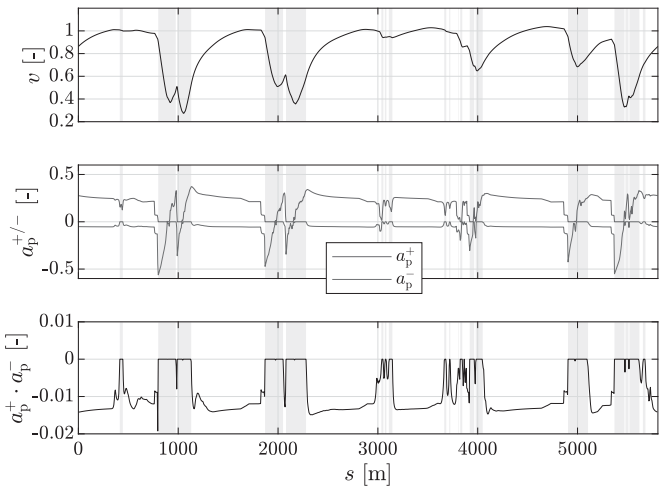

Fig. 12. Silverstone Circuit: Investigation of the split acceleration approach given in (31). Shown are the positive and negative components a_{p}^{+} and a_{p}^{-} of the propulsive acceleration, as well as their product. In the grip-limited regions highlighted in gray, complementarity holds, i.e., $a_{\mathrm{p}}^{+} \cdot a_{\mathrm{p}}^{-} = 0$.

In particular, the inequality constraints (5) and (13) linking velocity, lethargy and kinetic energy hold with equality in the optimal solution. Hence, the computed solution is physically meaningful.

Next, it is of interest to analyze the mathematical 'trick' of splitting up the propulsive acceleration in a positive and negative component by (29), (30) and (31). Fig. 12 shows the relevant optimization variables a_{p}^{+}, a_{p}^{-} and their product $a_{\mathrm{p}}^{+} \cdot a_{\mathrm{p}}^{-}$ together with the velocity profile as a function of distance. We note that a complementarity condition holds whenever the car is grip-limited, i.e., when the point $\{a_{\mathrm{lat}}(s), a_{\mathrm{p}}(s)\}$ lies on one of the half-ellipses evaluated at the velocity $v(s)$: The product of the two auxiliary variables is zero, meaning that at most one of them is non-zero. This is best explained using an example. Intuitively, after the apex of a corner it is optimal to accelerate at the grip limit. At a given velocity and lateral acceleration, the propulsive acceleration a_{p} should thus

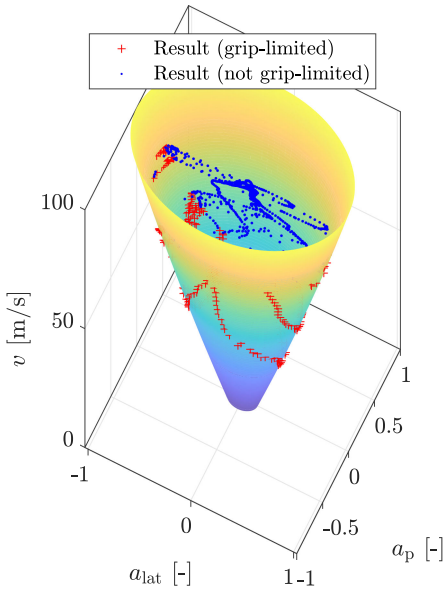

Fig. 13. Silverstone Circuit: Three-dimensional representation of the modeled performance envelope constraints (conic shape) and the optimal solution of Problem 1 (dots). The conic shape limits the feasible space for the triple $\{a_{\mathrm{lat}}, a_{\mathrm{p}}, v\}$. The grip-limited points are those that lie exactly on the boundary of the performance envelope, whilst all the other points lie inside.

be maximized. By (31), this means that a_{p}^{+} must be as large as permitted by the elliptic boundary (38), whilst a_{p}^{-} must be zero. With an analogous reasoning, one finds that when braking at the grip limit, $a_{\mathrm{p}}^{+} = 0$ must hold. Conversely, on the straights the achievable a_{p} is determined by the powertrain constraints, hence a^{+} and a^{-} can take arbitrary values within their respective feasible sets given by (29), (38) and (30), (39), as long as (31) is satisfied. On a sidenote, for the presented case study, a single elliptic constraint instead of two half-ellipses would not result in a significant loss of precision, since the two identified half-ellipses have a very similar shape. However, this proof-of-concept for the split acceleration approach paves the way for optimizing scenarios where the difference between acceleration and deceleration might be more pronounced.

To facilitate understanding, the implemented performance envelope constraints (29), (30), (31), (38), (39) are summarized in a three-dimensional graphical representation in Fig. 13. It depicts the resulting feasible space[2] for the triple $\{a_{\mathrm{lat}}, a_{\mathrm{p}}, v\}$. As one would intuitively expect, the performance envelope should be exploited as much as possible to minimize lap time. This is also exactly what an expert driver tries to achieve in a race car. In the graphic, points that lie on the boundary are marked as grip-limited. These correspond to the braking zones, the corners and the corner exits. For the other points, which mostly pertain to the power-limited straights, the performance envelope constraints are inactive.

[2]Actually, one would have to depict the four-dimensional feasible region for $\{a_{\mathrm{lat}}, a_{\mathrm{p}}, v, \tilde{E}_{\mathrm{kin}}\}$, since these variables are linked by the performance envelope constraints. However, we leverage the fact that (13) holds with equality in an optimal solution to achieve a three-dimensional plot.

D. Energy Management Strategies

In this section, we compare the energy management strategy obtained by solving Problem 1 with the one generated by the state-of-the art approach [29] that relies on a maximum velocity profile to capture the vehicle dynamics. It can be summarized as follows:

***Problem 3**:* With a maximum velocity profile, the minimum-lap-time energy management strategies are the solution of

$$\min \int_0^S \frac{\mathrm{d}t}{\mathrm{d}s}(s) \cdot \mathrm{d}s$$

subject to the constraints

Kinematics:	(5), (10), (11), (13),
Propulsive and drag forces:	(16), (17), (19), (20), (21),
Maximum velocity profile:	$\tilde{E}_{\text{kin}}(s) \leq \frac{1}{2} \cdot v_{\text{max}}^2(s) \, \forall s$ (22),
Powertrain (F1):	(47), (48), (49), (50), (52),
	(58), (59), (60), (61), (62).

The only difference to Problem 1 consists in replacing the performance envelope constraints with a maximum velocity profile. Hence, this comparison allows us to isolate the effect of the performance envelope on the energy management strategy and to validate the usefulness of the proposed optimization framework for energy management studies. The v_{max}-profile for the braking zones and corners is generated directly from the measured velocity by identifying the grip-limited regions, again for instance based on the driver's throttle pedal actuation. When solving Problem 3, the obtained velocity in the corners, where constraint (22) is active with $v(s) = v_{\text{max}}(s)$, thus corresponds exactly to the measured one.

The comparison is shown in Fig. 14 for the Silverstone Circuit. The specified values for the fuel consumption target $E_{\text{f,target}}$ in the terminal constraint (61) and the battery energy target $\Delta E_{\text{b,target}}$ in (62) were the same in both problems. Hence, the final values of fuel energy and battery energy are identical for both cases. Note that the achievable lap time strongly depends on the chosen consumption targets. Readers interested in that dependency are referred to [29]. For this comparison, we focus on the energy management strategy within the lap. We observe that it displays very similar features in both solutions. The engine is operated at full power along the entire straights in both solutions. The MGU-K operation is also very similar: As was established in previous works [29], [48], it is optimal to boost at the beginning of the straights in order to reach a high velocity quickly. Towards the end of the straights, when velocity is already high and not a lot of lap time could be gained anymore, it is optimal to switch off the electric motor, such that the battery energy consumption constraint (62) can be respected. In the grip-limited regions, the energy management task consists in balancing the power split between MGU-K and engine in a lap-time-optimal way, depending on the specified fuel and battery consumption targets: The MGU-K recuperates under braking, and in the corners, some load-point shifting [3] is done by using

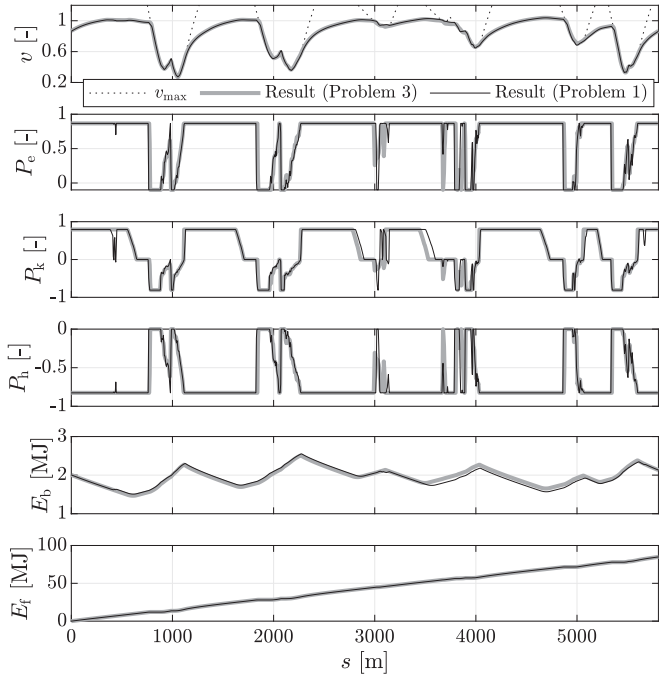

Fig. 14. Silverstone Circuit: Energy management comparison of the solution to Problem 1 with the proposed performance envelope constraints and the solution to Problem 3 with the state-of-the-art v_{max}-constraint. The plots show the most relevant trajectories in the context of the energy management, i.e., engine, MGU-K and MGU-H power, battery energy and fuel energy consumption.

part of the power generated by the engine to recharge the battery. Both solutions reflect this behavior. The small differences in the MGU-K operation (e.g., the earlier power cut at $s \approx 3500$ m) and in the engine/MGU-K interplay in part load operation stem from small discrepancies in the velocity profile. Indeed, the velocity that is feasible according to the performance envelope model and the v_{max}-profile slightly differ, and hence the feasible propulsive power is different at certain track locations. This can be very well observed, for instance, at $s \approx 400$ m. Here, for the solution of Problem 1, the grip limit prescribed by the performance envelope constraints briefly becomes active, requiring a drop in propulsive power. Given that in our powertrain model, the MGU-H power is coupled to the fuel power by (46), small differences between the two solutions occur where the engine power is also differing. Overall, these variations entailed by the limited accuracy of the convex performance envelope model do not lead to big deviations in the battery and fuel energy profiles. Therefore, the presented performance envelope is a valid tool for use in minimum-lap-time energy management optimization.

E. Adapting the Performance Envelope to Different Grip Levels

Our last case study demonstrates the effect of applying a shape-preserving scaling factor κ to the performance envelope. Given a performance envelope with parameters $P = \{c_1, c_2, c_3, r^+, r^-\}$, this means that the scaled set of parameters

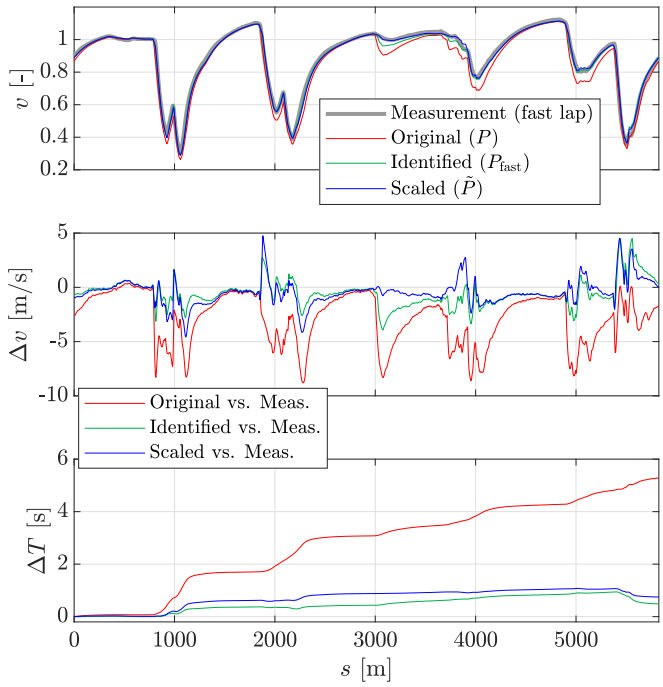

Fig. 15. Silverstone Circuit: Effect of applying a scaling factor to the performance envelope model. The measurement comes from a fast lap with low car mass and soft tires with increased grip. The 'Original' result is obtained by solving Problem 1 with the performance envelope parameters P identified with the data from a slower lap in Fig. 7. The 'Identified' result is generated with parameters P_{fast} that were identified with the measurement data from the fast lap by solving Problem 2. The 'Scaled' result is for parameters $\tilde{P}$ obtained by scaling P according to (65) with $\kappa = 1.14$.

$\tilde{P} = \{\tilde{c}_1, \tilde{c}_2, \tilde{c}_3, \tilde{r}^+, \tilde{r}^-\}$ is obtained as

$$\tilde{c}_1 = \boldsymbol{\kappa} \cdot c_1, \qquad \tilde{c}_2 = \boldsymbol{\kappa} \cdot c_2, \quad \tilde{c}_3 = \boldsymbol{\kappa} \cdot c_3,$$
$$\tilde{r}^+ = r^+, \qquad \tilde{r}^- = r^-. \tag{65}$$

Ultimately, this boils down to inflating ($\kappa > 1$) or shrinking ($\kappa < 1$) the originally identified half-ellipses. Fig. 15 shows a measurement recorded on the Silverstone Circuit during a lap with soft tires and with a low car mass due to low fuel load. The lap time was much lower compared to the measurement discussed in Section IV-A. In particular, the reduced inertia and increased tire grip led to higher lateral and longitudinal acceleration capabilities. When solving Problem 1 by applying the performance envelope parameters P identified in Fig. 7 for the slower lap, the obtained velocity profile is obviously mismatched. The apex speed in almost all corners is drastically too low, sometimes in excess of 5 m/s, and hence the lap time is more than 5 s too high. Using a set of parameters P_{fast} that was identified by applying the method described in Section III to the measurement data of the fast lap, the agreement is much better. The precision is similar to the results shown in Fig. 9 for the slower lap. Interestingly, using a set of parameters $\tilde{P}$ obtained from P by applying the scaling (65) with a well-chosen value of $\kappa = 1.14$, a comparable level of precision can be achieved. The lap time difference with respect to the measurement is reduced to less than 0.75 s. As one would expect intuitively, scaling the performance envelope P by a factor $\kappa > 1$ results in a faster lap time, due to the increased acceleration capabilities. With the exception of two braking zones, the difference in velocity comes down to similar values as observed for the parameters P_{fast}. This result suggests that on a given circuit, the effect of different tire grip levels and car mass can be simulated by applying a scaling factor to the performance envelope.

F. Advantages Compared to the State-of-the-art

Finally, we comment on the advantages of the novel formulation compared to the state-of-the-art maximum velocity profile approach [29]. First, both measuring a maximum velocity profile and synthesizing it in simulation requires some energy management controller, since the delivered propulsive power determines the velocity, which in turn defines the available tire grip of a race car with aerodynamic downforce. Hence, the energy management optimization cannot be studied in a truly independent manner with this method. By contrast, the new approach achieves this 'decoupling' because it does not require any a priori assumptions about the energy management. It thus allows to study the interaction between grip limits and optimal powertrain operation. Moreover, since the performance envelope model describes the physical link between longitudinal and lateral acceleration capabilities, the optimal energy management can be studied for different vehicle configurations: Indeed, as shown previously, modifying the parameters that describe the envelope leads to realistic results. Conducting such investigations with a maximum velocity profile requires a detailed vehicle dynamics simulation for each scenario beforehand, which can be impractical. Lastly, whilst the state-of-the-art method can exactly replicate the measured velocity in the grip-limited corners, other corners that were not grip-limited in the measurement are virtually non-existent for the optimization. However, the grip limit might be attained if, e.g., more available power led to a higher velocity, which can be relevant if investigations with different powertrain parameters are carried out. With the new formulation, all corners are included in the optimization via the path curvature. This difference is visible at $s \approx 400$ m in Fig. 14: For Problem 1 the grip limit is attained (because the performance envelope fit is somewhat underestimating the real grip), whereas the $v_{\max}$ profile does not imply a corner at this track location.

V. Conclusion

In this paper, we presented a convex model for the performance envelope of race car vehicle dynamics. The model is suitable for use in computationally efficient energy management optimization frameworks. Our approach does not optimize the driving path on the circuit, but we rather assume that the path is given in the form of a distance-based curvature trajectory. The model then consists of a grip limit in the form of two velocity-dependent half-ellipses that limit the achievable lateral acceleration and propulsive longitudinal acceleration in the g-g diagram. It is fully described by five fitting parameters and can be readily integrated into a previously developed second-order cone program which yields the energy management strategies for minimum lap time. Our case study for a hybrid-electric F1 car on

the Silverstone circuit shows that the method is accurate enough for the intended purpose. Indeed, comparing the optimization results to the measurement data, we found that the difference between the optimal velocity profile and the measured velocity is contained to ± 2 m/s at most track locations (the few exceptions stemming from the discretization of the problem), whilst the lap time difference is only 0.5 s. Similar results were obtained in a second case study for the Spa-Francorchamps Circuit, which evidences that the method is easily applicable to different scenarios. What is more, a comparison with the state-of-the-art framework for lap-time-optimal energy management resulted in very similar power and energy consumption trajectories. This validates the presented model for optimizing the energy management of hybrid-electric race cars. Finally, we showed that the performance envelope can be scaled to simulate different grip levels on a given race circuit.

Certainly, the convex performance envelope model can be included with minimal effort in previously developed optimization frameworks that so far have relied on a maximum velocity profile approach, such as [30], [33], [49]. Further research could investigate other shapes for the fit of the performance envelope boundary, for instance a set of piece-wise affine constraints. An increase in precision could possibly be achieved by identifying the performance envelope separately for each corner. Moreover, a simulation framework for causal energy management controllers in racing applications could be developed, using the proposed performance envelope model to approximate the vehicle dynamics. The scaling properties of the model could be exploited in a model predictive control framework, in order to adapt the energy management to varying grip levels.

APPENDIX

A. Second-order Cone Program

A second-order cone program is a particular type of a convex optimization problem that can be stated in the following form [42]:

$$\min_{x} \quad f^{\top} \cdot x \tag{66}$$

$$\text{subject to} \quad \|A_i \cdot x + b_i\|_2 \leq c_i^{\top} \cdot x + d_i \qquad i = 1, \ldots, m \tag{67}$$

$$F \cdot x = g \tag{68}$$

The vector $x \in \mathbb{R}^n$ is the optimization variable, and the matrices have the dimensions $A_i \in \mathbb{R}^{n_i \times n}$ and $F \in \mathbb{R}^{p \times n}$. The constraints (67) are called second-order cone constraints. Linear inequality constraints are a special form of second-order cone constraints. Indeed, with $A_i = 0 \quad \forall\, i$, the above problem reduces to a linear program. Like linear programs, second-order cone programs can be solved in polynomial time with interior point methods and optimality guarantees [50].

ACKNOWLEDGMENT

We thank Ferrari S.p.A. for supporting this project. Moreover, we are grateful to Tammo Zobel and Camillo Balerna for their constructive feedback on earlier versions of this article. We also want to thank Dr. Ilse New for proofreading this paper.

REFERENCES

[1] R. S. Rice, "Measuring car-driver interaction with the g-g diagram," SAE Int., Warrendale, PA, USA, Tech. Paper 730018, 1973.
[2] J. Katz, *Race Car Aerodynamics: Designing for Speed*, Cambridge, U.K.: R. Bentley, 1995.
[3] A. Sciarretta and L. Guzzella, *Vehicle Propulsion Systems*, *3rd ed*. Berlin, Germany: Springer, 2013.
[4] FIA, " Jun. 2021 Formula One Technical Regulations" Fédération Internationale de l'Automobile, Paris, France, Tech. Rep., no. 10, 2021.
[5] FIA, "2022 Le Mans Hypercar Technical Regulations" Fédération Internationale de l'Automobile, Paris, France, Tech. Rep., Dec. 2021.
[6] FIA, "2021-2022 Formula E World Championship Technical Regulations" Fédération Internationale de l'Automobile, Tech. Rep., vol. 6, Paris, France, Nov. 2021.
[7] W. F. Milliken *et al.*, *Race Car Vehicle Dynamics*, vol. 400. Warrendale, PA, USA: Society of Automotive Engineers, 1995.
[8] M. Yamakado and M. Abe, "An experimentally confirmed driver longitudinal acceleration control model combined with vehicle lateral motion," *Veh. Syst. Dyn.*, vol. 46, no. S1, pp. 129–149, 2008.
[9] A. M. Daher, C. R. Bardawil, and N. A. Daher, "Vehicle stability based on g-g diagram through braking and driveline," in *Proc. IEEE Amer. Control Conf.*, 2017, pp. 309–314.
[10] A. Tremlett, F. Assadian, D. Purdy, N. Vaughan, A. Moore, and M. Halley, "Quasi-steady-state linearisation of the racing vehicle acceleration envelope: A limited slip differential example," *Veh. Syst. Dyn.*, vol. 52, no. 11, pp. 1416–1442, 2014.
[11] K. Kritayakirana and J. C. Gerdes, "Autonomous cornering at the limits: Maximizing a "gg" diagram by using feedforward trail-braking and throttle-on-exit," *IFAC Proc. Volumes*, vol. 43, no. 7, pp. 548–553, 2010.
[12] M. Fu, J. Ni, X. Li, and J. Hu, "Path tracking for autonomous race car based on G-G diagram," *Int. J. Automot. Technol.*, vol. 19, no. 4, pp. 659–668, 2018.
[13] F. Biral and R. Lot, "An interpretative model of g-g diagrams of racing motorcycle," in *Proc. 3rd ICMEM Int. Conf. Mech. Eng. Mechanics*. Beijing, Repubblica Popolare Cinese, Ottobre, 2009, pp. 21–23.
[14] B. Siegler, A. Deakin, and D. Crolla, "Lap time simulation: Comparison of steady state, quasi-static and transient racing car cornering strategies," *SAE Trans.*, vol. 109, pp. 2575–2581, 2000.
[15] T. Völkl, M. Muehlmeier, and H. Winner, "Extended steady state lap time simulation for analyzing transient vehicle behavior," *SAE Int. J. Passenger Cars- Mech. Syst.*, vol. 6, no. 2013-01-0806, pp. 283–292, 2013.
[16] D. Brayshaw and M. Harrison, "A quasi steady state approach to race car lap simulation in order to understand the effects of racing line and centre of gravity location," *Proc. Inst. Mech. Engineers, Part D: J. Automobile Eng.*, vol. 219, no. 6, pp. 725–739, 2005.
[17] D. Casanova, "On minimum time vehicle manoeuvring: The theoretical optimal lap," Ph.D. dissertation, Cranfield University, Cranfield, Bedfordshire, England, 2000.
[18] D. P. Kelly, "Lap time simulation with transient vehicle and tyre dynamics," Ph.D. dissertation, Cranfield University, Cranfield, Bedfordshire, England, 2008.
[19] G. Perantoni and D. J. Limebeer, "Optimal control for a formula one car with variable parameters," *Veh. System Dyn.*, vol. 52, no. 5, pp. 653–678, 2014.
[20] A. Rucco, G. Notarstefano, and J. Hauser, "An efficient minimum-time trajectory generation strategy for two-track car vehicles," *IEEE Trans. Control Syst. Technol.*, vol. 23, no. 4, pp. 1505–1519, Jul. 2015.
[21] R. Lot and N. Dal Bianco, "Lap time optimisation of a racing go-kart," *Veh. Syst. Dyn.*, vol. 54, no. 2, pp. 210–230, 2016.
[22] N. Dal Bianco, E. Bertolazzi, F. Biral, and M. Massaro, "Comparison of direct and indirect methods for minimum lap time optimal control problems," *Veh. Syst. Dyn.*, vol. 57, no. 5, pp. 665–696, 2019.
[23] T. Lipp and S. Boyd, "Minimum-time speed optimisation over a fixed path," *Int. J. Control*, vol. 87, no. 6, pp. 1297–1311, 2014.
[24] J. P. Timings and D. J. Cole, "Minimum maneuver time calculation using convex optimization," *J. Dynamic Syst., Measurement, Control*, vol. 135, no. 3, 2013, Art. no. 031015.

[25] N. R. Kapania, J. Subosits, and J. Christian Gerdes, "A sequential two-step algorithm for fast generation of vehicle racing trajectories," *J. Dynamic Syst., Meas., Control*, vol. 138, no. 9, 2016, Art. no. 091005.
[26] R. Verschueren, S. De Bruyne, M. Zanon, J. V. Frasch, and M. Diehl, "Towards time-optimal race car driving using nonlinear MPC in real-time," in *Proc. 53rd IEEE Conf. Decis. Control*, 2014, pp. 2505–2510.
[27] R. Verschueren, M. Zanon, R. Quirynen, and M. Diehl, "Time-optimal race car driving using an online exact hessian based nonlinear MPC algorithm," in *Proc. IEEE Eur. Control Conf.*, 2016, pp. 141–147.
[28] N. R. Kapania and J. C. Gerdes, "Learning at the racetrack: Data-driven methods to improve racing performance over multiple laps," *IEEE Trans. Veh. Technol.*, vol. 69, no. 8, pp. 8232–8242, Aug. 2020.
[29] S. Ebbesen, M. Salazar, P. Elbert, C. Bussi, and C. H. Onder, "Time-optimal control strategies for a hybrid electric race car," *IEEE Trans. Control Syst. Technol.*, vol. 26, no. 1, pp. 233–247, Jan. 2018.
[30] P. Duhr, G. Christodoulou, C. Balerna, M. Salazar, A. Cerofolini, and C. H. Onder, "Time-optimal gearshift and energy management strategies for a hybrid electric race car," *Appl. Energy*, vol. 282, 2020, Art. no. 115980.
[31] O. Borsboom, C. A. Fahdzyana, T. Hofman, and M. Salazar, "A convex optimization framework for minimum lap time design and control of electric race cars," *IEEE Trans. Veh. Technol.*, vol. 70, no. 9, pp. 8478–8489, Sep. 2021.
[32] A. Locatello, M. Konda, O. Borsboom, T. Hofman, and M. Salazar, "Time-optimal control of electric race cars under thermal constraints," in *Proc. IEEE Eur. Control Conf.*, 2021, pp. 905–912.
[33] C. Balerna *et al.*, "Time-optimal low-level control and gearshift strategies for the Formula 1 hybrid electric powertrain," *Energies*, vol. 14, no. 171, pp. 1–30, 2021.
[34] M. Salazar, P. Duhr, C. Balerna, L. Arzilli, and C. H. Onder, "Minimum lap time control of hybrid electric race cars in qualifying scenarios," *IEEE Trans. Veh. Technol.*, vol. 68, no. 8, pp. 7296–7308, Aug. 2019.
[35] D. J. Limebeer, G. Perantoni, and A. V. Rao, "Optimal control of formula one car energy recovery systems," *Int. J. Control*, vol. 87, no. 10, pp. 2065–2080, 2014.
[36] T. Herrmann, F. Christ, J. Betz, and M. Lienkamp, "Energy management strategy for an autonomous electric racecar using optimal control," in *Proc. IEEE Intell. Transp. Syst. Conf.*, 2019, pp. 720–725.
[37] T. Herrmann, F. Passigato, J. Betz, and M. Lienkamp, "Minimum race-time planning-strategy for an autonomous electric racecar," in *Proc. IEEE 23rd Int. Conf. Intell. Transp. Syst.*, 2020, pp. 1–6.
[38] X. Liu, A. Fotouhi, and D. J. Auger, "Optimal energy management for formula-e cars with regulatory limits and thermal constraints," *Appl. Energy*, vol. 279, 2020, Art. no. 115805.
[39] R. Lot and S. A. Evangelou, "Lap time optimization of a sports series hybrid electric vehicle," in *Proc. World Congr. Eng.*, 2013, pp. 1–6.
[40] S. East and M. Cannon, "Fast optimal energy management with engine on/off decisions for plug-in hybrid electric vehicles," *IEEE Control Syst. Lett.*, vol. 3, no. 4, pp. 1074–1079, Oct. 2019.
[41] S. Broere and M. Salazar, "Minimum-lap-time control strategies for all-wheel drive electric race cars via convex optimization," 2021, *arXiv:2111.04650*.
[42] S. Boyd and L. Vandenberghe, *Convex Optimization*. Cambridge, U.K.: Cambridge Univ. Press, 2004.
[43] M. Mitschke and H. Wallentowitz, *Dynamik Der Kraftfahrzeuge*, vol. 4. Berlin, Germany: Springer, 1972.
[44] N. Murgovski, L. Johannesson, X. Hu, B. Egardt, and J. Sjöberg, "Convex relaxations in the optimal control of electrified vehicles," in *Proc. IEEE Amer. Control Conf.*, 2015, pp. 2292–2298.
[45] E. Velenis, P. Tsiotras, and J. Lu, "Modeling aggressive maneuvers on loose surfaces: The cases of trail-braking and pendulum-turn," in *Proc. IEEE Eur. Control Conf.*, 2007, pp. 1233–1240.
[46] J. Lofberg, "YALMIP: A toolbox for modeling and optimization in MATLAB," in *Proc. IEEE Int. Conf. Robot. Automat.*, 2004, pp. 284–289.
[47] A. Domahidi, E. Chu, and S. Boyd, "ECOS: An SOCP solver for embedded systems," in *Proc. Eur. Control Conf.*, 2013, pp. 3071–3076.
[48] M. Salazar, P. Elbert, S. Ebbesen, C. Bussi, and C. H. Onder, "Time-optimal control policy for a hybrid electric race car," *IEEE Trans. Control Syst. Technol.*, vol. 25, no. 6, pp. 1921–1934, Nov. 2017.
[49] O. Borsboom, C. A. Fahdzyana, and M. Salazar, "Time-optimal control strategies for electric race cars with different transmission technologies," in *Proc. IEEE Veh. Power Propulsion Conf.*, 2020, pp. 1–5.
[50] F. Alizadeh and D. Goldfarb, "Second-order cone programming," *Math. Program.*, vol. 95, no. 1, pp. 3–51, 2003.

Pol Duhr received the B.Sc. and M.Sc. degrees in mechanical engineering in 2015 and 2018, respectively, from ETH Zürich, Zürich, Switzerland, where he is currently working toward the Ph.D. degree with the Institute for Dynamic Systems and Control. His research focuses on the time-optimal control of race car powertrains. He was awarded by the ETH Medal for the Master thesis on the control of the Formula 1 power unit. He was the recipient of the Student Award at the 2021 FISITA World Congress.

Ashwin Sandeep received the Bachelor of Engineering (Industrial) in mechanical engineering from the University of Leeds, Leeds, U.K., in 2020. He is currently working toward the M.Sc. degree in mechanical engineering with ETH Zürich, Switzerland. He held various roles with the Leeds Formula Student Team. Mr. Sandeep was the recipient of the University of Leeds Beaumont Award 2020 for excellence in undergraduate research.

Alberto Cerofolini received the M.Sc. degree in mechanical engineering and the Ph.D. degree in mechanics and engineering advanced science from the Università di Bologna, Bologna, Italy, in 2009 and 2014, respectively. He currently holds a position as Power Unit Performance Engineer with the Power Unit Performance and Control Strategies Group of the Formula 1 team Scuderia Ferrari. His research focuses on lap-time-optimal and robust control strategies for the energy management of the Formula 1 car.

Christopher H. Onder received the Diploma and Ph.D. degree in mechanical engineering from ETH Zürich, Zürich, Switzerland. He is currently a Professor with the Institute for Dynamic Systems and Controls, ETH Zürich. He has authored or coauthored numerous articles and a book on modeling and control of engine systems. Prof. Dr. Onder was the recipient of the BMW Scientific Award, ETH Medal, Vincent Bendix Award, and Watt d'Or Energy Prize.